The Astrophysical Journal, 850:154 (7pp), 2017 December 1 https://doi.org/10.3847/1538-4357/aa9567

Phase Offsets and the Energy Budgets of Hot Jupiters

Joel C. Schwartz[1,2,3,6], Zane Kashner[4], Diana Jovmir[2,5,6], and Nicolas B. Cowan[1,2,6]
[1] Department of Earth & Planetary Sciences, McGill University, 3450 rue University, Montreal, QC, H3A 0E8, Canada; joel.schwartz@mail.mcgill.ca
[2] Department of Physics, McGill University, 3600 rue University, Montreal, QC, H3A 2T8, Canada
[3] Department of Physics & Astronomy, Northwestern University, 2145 Sheridan Road, Evanston, IL 60208, USA
[4] Department of Mathematics, Stanford University, 450 Serra Mall, Stanford, CA 94305, USA
[5] Department of Mathematics & Statistics, Université de Montréal, 2920 chemin de la Tour, Montreal, QC, H3T 1J4, Canada
Received 2017 March 19; revised 2017 October 20; accepted 2017 October 20; published 2017 November 28

Abstract

Thermal phase curves of short-period planets on circular orbits provide joint constraints on the fraction of incoming energy that is reflected (Bond albedo) and the fraction of absorbed energy radiated by the night hemisphere (heat recirculation efficiency). Many empirical studies of hot Jupiters have implicitly assumed that the dayside is the hottest hemisphere and the nightside is the coldest hemisphere. For a given eclipse depth and phase amplitude, an orbital lag between a planet's peak brightness and its eclipse—a phase offset—implies that planet's nightside emits greater flux. To quantify how phase offsets impact the energy budgets of short-period planets, we compile all infrared observations of the nine planets with multi-band eclipse depths and phase curves. Accounting for phase offsets shifts planets to lower Bond albedo and greater day–night heat transport, usually by $\lesssim 1\sigma$. For WASP-12b, the published phase variations have been analyzed in two different ways, and the inferred energy budget depends sensitively on which analysis one adopts. Our fiducial scenario supports a Bond albedo of $0.27^{+0.12}_{-0.13}$, significantly higher than the published optical geometric albedo, and a recirculation efficiency of $0.03^{+0.07}_{-0.02}$, following the trend of larger day–night temperature contrast with greater stellar irradiation. If instead we adopt the alternative analysis, then WASP-12b has a Bond albedo consistent with zero and a much higher recirculation efficiency. To definitively determine the energy budget of WASP-12b, new observational analyses will be necessary.

Key words: infrared: planetary systems – methods: statistical – planets and satellites: atmospheres

1. Introduction

Short-period planets on circular orbits are expected to have permanent day and night hemispheres. Only the dayside absorbs stellar radiation, but if the planet has an atmosphere, then some energy can be moved to the nightside. The process can be described by Bond albedo, $A_B \in [0, 1]$, the fraction of incident flux the planet reflects, and heat recirculation efficiency, $\varepsilon \in [0, 1]$, the fraction of absorbed energy transported from day to night. One can constrain both parameters using the planet's day and night effective temperatures, T_d and T_n, respectively.

A notional thermal phase curve for a planet is shown by the orange line in Figure 1. The flux varies because one sees different planetary phases over time, from the nightside at transit to the dayside at eclipse. By combining the eclipse depth, phase variations, transit depth, and stellar spectrum, one can infer the planet's day and night brightness temperatures. By combining brightness temperatures at many wavelengths, one can estimate effective temperatures of a planet's day and night hemispheres.

Many previous studies of hot Jupiters have neglected phase offsets, instead assuming that the dayside is the hottest hemisphere and the nightside is the coolest (Cowan & Agol 2011b; Perez-Becker & Showman 2013; Schwartz & Cowan 2015; Komacek et al. 2017). This is denoted by the gray line in Figure 1. Because those authors used the actual eclipse depths, the dayside estimates were accurate; but by adopting the published phase amplitudes and assuming that the nightside was the coolest hemisphere, they underestimated the nightside brightness and hence temperature.

[6] McGill Space Institute; Institute for Research on Exoplanets.

In Section 2.1, we review the compiled data for our energy budget model, including new observations at thermal wavelengths. In Section 2.2, we describe how we use phase offsets in this model, then fit the Bond albedo and recirculation efficiency of nine short-period giant planets. We discuss our results and conclude in Section 3.

2. Energy Balance

For transiting planets, one infers Bond albedo and heat recirculation efficiency from infrared observations by estimating effective temperatures for the planet's day and nightsides. This is described by Equations (4)–(6) of Cowan & Agol (2011b), which were used and expanded on by Schwartz & Cowan (2015).

2.1. Data

Data for these studies were collected by reviewing published papers and searching both exoplanet.eu (Schneider et al. 2011) and exoplanets.org (Han et al. 2014). We start with the six planets in Table 2 of Schwartz & Cowan (2015) that have thermal eclipses and phase amplitudes (at wavelengths longward of 0.8 μm): HD 149026b, HD 189733b, HD 209458b, WASP-12b, WASP-18b, and WASP-43b. Then we add WASP-14b (Wong et al. 2015), HAT-P-7b, and WASP-19b (Wong et al. 2016) to our sample. We also incorporate new data from Zhou et al. (2015), Evans et al. (2015), and Line et al. (2016).

We collect first-order phase offsets (Sections 2.2 and 2.2.1) from Knutson et al. (2009a, 2009b) and Wong et al. (2015, 2016). Knutson et al. (2009a) concluded the offset they found was not statistically significant, so we use their largest uncertainty ($72° \pm 61°$). Phase offsets through *second* order

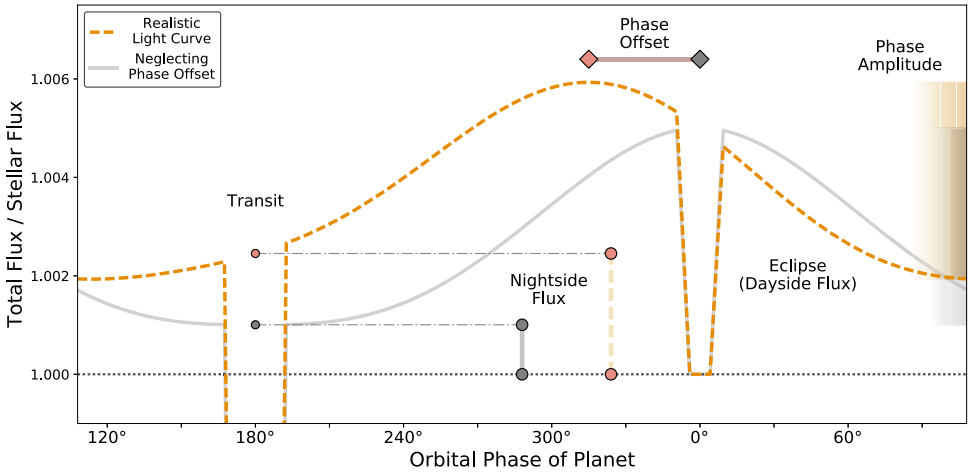

Figure 1. Light curves of a transiting planet with a given eclipse depth and phase amplitude. The horizontal dotted black line denotes the unobscured stellar flux. The dashed orange curve has a non-zero phase offset. If one neglects this offset, then one is instead adopting the gray curve, as was done in previous energy budget studies (e.g., Schwartz & Cowan 2015). To the lowest order, the planet's nightside flux is the eclipse depth minus the peak-to-trough phase amplitude, but this is only exact if the planet exhibits no phase offset. For a fixed eclipse depth and phase amplitude, accounting for a non-zero phase offset (dashed orange curve) will lead one to infer greater nightside flux.

come from Cowan et al. (2012), Knutson et al. (2012), Maxted et al. (2013), Zellem et al. (2014), and Stevenson et al. (2014c, 2017). However, the second-order components in Zellem et al. (2014) were found to be unnecessary, and those at 4.5 micron in Cowan et al. (2012) are disputed, so we use neither in our fits. Also, Cowan et al. (2012) reported two sets of fit parameters for WASP-12b based on different models for detector systematics[7]—we use parameters from their preferred polynomial model but test the other scenario in Section 3.1.[8] All nine planets in our study have non-zero offsets in at least one waveband.

2.2. Model

We take an energy balance approach to interpreting thermal phase variations (e.g., Cowan & Agol 2011b): we compare the radiation going into and coming out from a planet to infer bulk energetics of that planet's atmosphere.

For our study, we use the energy balance model described in Section 3.1 of Schwartz & Cowan (2015), which accounts for uncertainties in system parameters, as well as reflected light contamination, meridional heat transport, and other sources of uncertainty. Those authors treated stars as blackbodies; we estimate better stellar brightness temperatures for each observation by using BT-NextGen spectra (Allard et al. 2012). Then we use our compiled data to calculate the relative intensity of planets and their host stars at each observed wavelength. In Cowan & Agol (2011b) and Schwartz & Cowan (2015), this nightside intensity ratio, $\psi_n(\lambda)$, is defined as

$$\psi_n(\lambda) = \frac{\delta_{ecl} - \delta_{var}}{\delta_{tr}}, \quad (1)$$

where δ_{ecl} is the eclipse depth, δ_{var} is the peak-to-trough phase amplitude of the full light curve, and δ_{tr} is the transit depth. This is exact only when an observation has no phase offset (e.g., gray curve in Figure 1).

More generally, one can model the flux F_p from a planet as a Fourier series:

$$F_p(\phi) \approx F_0 + \sum_{k=1}^{k_{max}} \frac{\delta_k}{2} \cos\left[k(\phi - \phi_k)\right], \quad (2)$$

where ϕ is the planet's orbital phase (0° at eclipse), and δ_k and ϕ_k are the phase amplitude and offset of order k, respectively. Six of the ten published papers with phase offsets use phase curves like this to model their data; we convert parameters from the other studies into the form of Equation (2). We then modify Equation (1) to

$$\psi'_n(\lambda) = \frac{\delta_{ecl} - [F_p(0°) - F_p(180°)]}{\delta_{tr}}. \quad (3)$$

For a given eclipse depth and phase amplitude, this increases the brightness of a planet's nightside when there is an offset and reduces to Equation (1) otherwise (cf. dashed orange and solid gray curves in Figure 1).

If zonal heat advection is the dominant process governing thermal phase curves, then there should be a one-to-one correspondence between the amplitudes and phase offsets of bolometric phase curves. This was first noted by Crossfield (2015) and is discussed in Appendix A. In practice, though, we do not yet have bolometric phase curves for any exoplanets: <50% of the dayside flux and much less of the nightside flux has been captured for most hot Jupiters (Section 2.3 of Schwartz & Cowan 2015). Moreover, we suspect that clouds and magnetic fields might influence hot Jupiter phase curves (Parmentier et al. 2016; Rogers 2017). We therefore take the published phase amplitudes and offsets at face value and do not worry about whether they are consistent with the zonal advection hypothesis. However, we do establish that the published *uncertainties* on phase amplitudes and offsets are self-consistent (Appendix B).

[7] Stevenson et al. (2014a) fit eclipse depths for WASP-12b but not phase parameters, so we do not use their values in our analysis.

[8] WASP-12 has binary companion stars that affect photometry of the system (Bechter et al. 2014). We use dilution factors from Stevenson et al. (2014b) to correct observations of WASP-12b when appropriate.

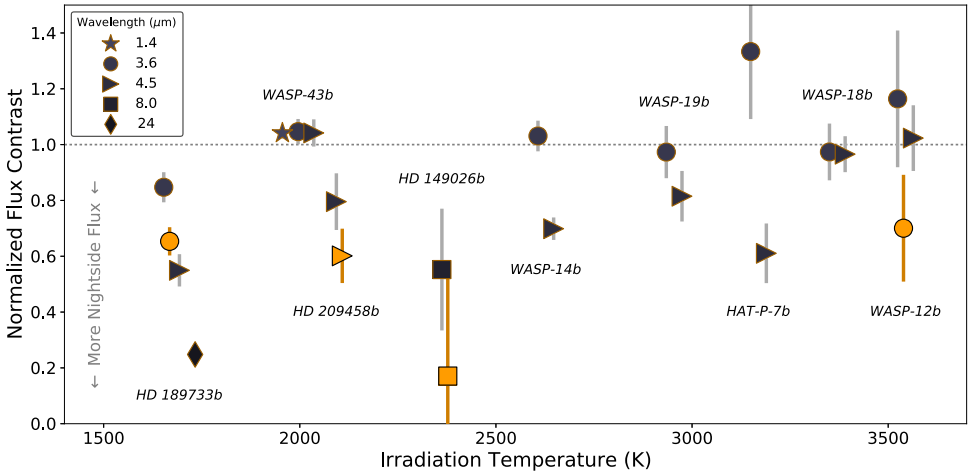

Figure 2. Following Perez-Becker & Showman (2013), we plot normalized day–night flux contrast, $(F_{\rm day} - F_{\rm night})/F_{\rm day}$, vs. irradiation temperature, $T_0 \equiv T_* \sqrt{R_*/a}$, where T_* is the stellar effective temperature, R_* is the stellar radius, and a is the planet's semimajor axis. Each marker represents a published observation with a phase offset, and the vertical lines show 1σ uncertainties (if larger than the marker). The horizontal dotted line shows where the nightside emits no flux. We label the nine planets in our sample and shift markers horizontally for clarity. Dark markers with gray lines show the flux contrasts when neglecting phase offsets (Perez-Becker & Showman 2013), while orange symbols show the more accurate contrasts accounting for offsets—we plot the corrected flux contrast if it changes by $\geqslant$0.05. For most observations, inferred nightside flux only changes a little after including phase offsets, but in a few cases it increases more significantly.

2.2.1. Second-order Phase Variations

The light curves in Figure 1 are composed of multiple modes, i.e., several δ_k are non-zero in Equation (2). When we use the semi-analytic energy balance model of Cowan & Agol (2011a) to calculate a planet's flux (Appendices A and C), the resulting light curves always have non-zero harmonics. We fit these synthetic light curves up to fourth order and find that $\delta_2/\delta_1 \approx 0.1$–$0.2$, $\delta_3 \approx 0$ (as expected for edge-on orbits; Cowan et al. 2013), and $\delta_4/\delta_1 \lesssim 0.01$. We repeat these fits on light curves of HD 189733b, HD 209458b, and WASP-43b from a global circulation model (Zhang et al. 2017) and obtain very similar results.

Published phase curves have $\delta_2/\delta_1 \lesssim 0.15$ (e.g., Maxted et al. 2013; Stevenson et al. 2017). Only for the 4.5 μm phase curve of WASP-12b is the second-order amplitude greater ($\sim$0.6; Cowan et al. 2012), but the authors note that it could not be due to planetary temperature patterns, so we neglect this second-order component. In any case, we use all published phase amplitude and offset data for Equation (3) so that our results are as robust as possible. First-order phase curves should be accurate to $\sim$15%, while those reported to second order should be good to $\sim$1%.

2.3. The Effect of Phase Offsets

We reproduce two figures that have previously been used to explore trends in the energy balance of short-period planets, but now we account for phase offsets.

Figure 2 is similar to Figure 1 from Perez-Becker & Showman (2013). For all infrared observations with a phase offset, we plot the flux contrast when neglecting those offsets as dark markers with 1σ uncertainties. If accounting for the offset decreases the contrast by at least 0.05, we also show an orange marker. Most nightside fluxes are only modestly affected by phase offsets. But, the 3.6 μm contrasts for HD 189733b and WASP-12b change significantly when phase offsets are accounted for. Because Perez-Becker & Showman (2013) ignored phase offsets (their data looks like the gray symbols in our plot), they over-estimated the day–night temperature contrast for those planets.

Figure 3 is similar to Figure 5 of Schwartz & Cowan (2015). To determine the Bond albedo and recirculation efficiency of each planet, we use either Equations (1) or (3) to calculate dayside and nightside brightness temperatures of planets. Next, we estimate a planet's day and nightside effective temperatures as the weighted average of its brightness temperatures. We then calculate χ^2 on a grid of $A_{\rm B}$ and ε. The 1σ regions are shown in Figure 3 and colored by irradiation temperature. Following Figure 1, light solid curves do not account for phase offsets while dashed curves do. We list our fit parameters for the dashed regions in Table 1 and the corresponding changes from the light solid regions in Table 2. The dayside and nightside temperatures we report are all *apparent* effective temperatures: the true effective temperatures of the day and night hemispheres are likely lower and higher, respectively, as discussed in Appendix C.

3. Discussion and Conclusions

In Figure 3, nightside temperatures increase toward the upper left. As expected, our fits accounting for phase offsets move to the upper left, with lower Bond albedo and higher day–night heat transport (updated parameters listed in Table 1). In most cases, the more accurate energy budget constraints agree at the 1σ level with previous estimates that neglected phase offsets (Table 2).[9]

The exception is the inferred nightside temperature for WASP-12b, which Table 2 shows is significantly hotter when including phase offsets. Our fitted Bond albedo for WASP-12b is also significantly higher than the planet's optical geometric albedo reported by Bell et al. (2017).[10] This is the same tension Schwartz & Cowan (2015) found when analyzing infrared and optical measurements of HD 189733b and HD 209458b.

For WASP-43b, we find that the upper limit on its nightside temperature increases by about an order of magnitude, up from $T_{\rm n} < 39$ K at 1σ when neglecting phase offsets.[11] Besides

[9] Although we used second-order phase curves where available, we obtain similar results using only first-order phase curves.

[10] Bell et al. (2017) cited the dayside temperature and Bond albedo for WASP-12b from an earlier version of this manuscript.

[11] Since the submission of this manuscript, Keating & Cowan (2017) suggested that the nightside temperature of WASP-43b is in fact in line with HD 209458b.

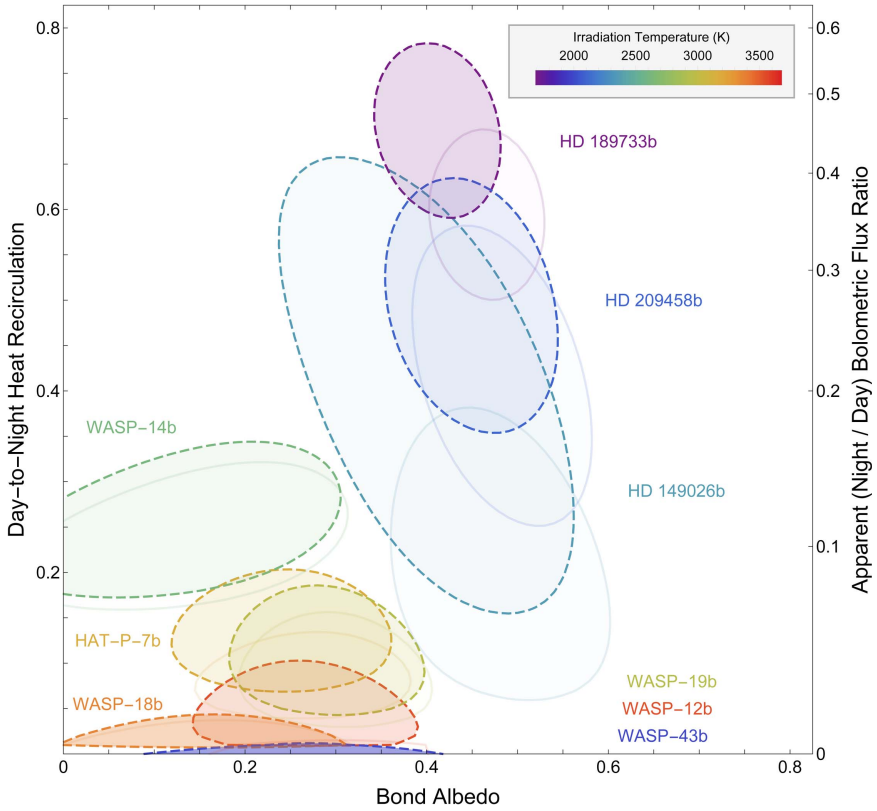

Figure 3. Fitted Bond albedo (A_B) and day–night heat recirculation efficiency (ε) for nine short-period planets with infrared eclipse and phase data, improved from Schwartz & Cowan (2015). We also show the apparent bolometric flux ratio for a planet's night and dayside on the right axis (Appendix C). Light solid curves show the 1σ regions when neglecting phase offsets, while dashed curves show the more accurate energy budgets accounting for offsets. The color scale shows irradiation temperature; shading is inversely related to the area of the 1σ region such that tighter fits are darker. The solid curve for WASP-43b is on the bottom axis (its nightside has zero flux if phase offsets are neglected). Every inferred Bond albedo and recirculation efficiency changes by $\lesssim 1\sigma$ when accounting for phase offsets (but see Section 3.1).

Table 1
Fitted Energy Budgets Accounting for Phase Offsets

Planet	T_d (K)	T_n (K)	A_B	ε
HAT-P-7b	2612 ± 93	1236 ± 178	$0.25^{+0.11}_{-0.13}$	$0.12^{+0.08}_{-0.05}$
HD 149026b	1737 ± 75	1127 ± 251	$0.43^{+0.13}_{-0.19}$	$0.37^{+0.29}_{-0.22}$
HD 189733b	1163 ± 37	953 ± 44	$0.41^{+0.07}_{-0.07}$	$0.69^{+0.09}_{-0.1}$
HD 209458b	1483 ± 51	1058 ± 92	$0.46^{+0.08}_{-0.11}$	$0.49^{+0.15}_{-0.14}$
WASP-12b	2939 ± 94	962 ± 354	$0.27^{+0.12}_{-0.13}$	$0.03^{+0.07}_{-0.02}$
WASP-14b	2193 ± 116	1262 ± 95	$0.14^{+0.16}_{-0.14}$	$0.25^{+0.09}_{-0.08}$
WASP-18b	2905 ± 111	662 ± 378	$0.16^{+0.15}_{-0.16}$	$0.01^{+0.03}$
WASP-19b	2407 ± 82	1069 ± 200	$0.3^{+0.1}_{-0.12}$	$0.1^{+0.09}_{-0.06}$
WASP-43b	1667 ± 56	<430 (1σ)	$0.27^{+0.15}_{-0.18}$	$0^{+0.01}$

Table 2
Change in Parameters after Using Phase Offsets

Planet	ΔT_n (K)	ΔA_B	$\Delta\varepsilon$
HAT-P-7b	146 ± 246	-0.02 ± 0.17	0.04 ± 0.08
HD 149026b	214 ± 333	-0.06 ± 0.2	0.19 ± 0.3
HD 189733b	56 ± 62	-0.06 ± 0.09	0.1 ± 0.13
HD 209458b	64 ± 157	-0.03 ± 0.14	0.09 ± 0.22
WASP-12b	646 ± 487	-0.02 ± 0.17	0.03 ± 0.05
WASP-14b	27 ± 134	0 ± 0.22	0.02 ± 0.12
WASP-18b	7 ± 516	-0.01 ± 0.22	0 ± 0.02
WASP-19b	72 ± 290	-0.01 ± 0.15	0.02 ± 0.1
WASP-43b	<432 (1σ)	0 ± 0.23	0 ± 0.01

WASP-12b and WASP-43b, HD 189733b has the most significant changes to its energy budget constraints in Table 2.

3.1. Energy Budget of WASP-12b

The dashed region for WASP-12b in Figure 3 agrees well with Figure 10 from Cowan et al. (2012). This alone is interesting: we use more eclipse measurements of the planet, correct for binary companion stars diluting those measurements (Stevenson et al. 2014b), take higher-order phase components into account, and use phase offsets.

As stated in Section 2.1, Cowan et al. (2012) fit their light curves of WASP-12b with two models for detector systematics, polynomial and Gaussian decorrelation. In particular, the polynomial model gives a significantly larger phase amplitude at 4.5 μm, plus a shallower eclipse depth and much larger phase offset ($-53^\circ \pm 7^\circ$ versus $0^\circ \pm 29^\circ$) at 3.6 μm. We use the polynomial values because the authors argue that their Gaussian decorrelation method removes a lot of the planet's phase signal. But it is difficult to decide which systematics model works better using just goodness-of-fit. We therefore fit an alternate energy budget for WASP-12b.

We repeat our analysis on WASP-12b using parameters from the Gaussian decorrelation model in Cowan et al. (2012) and infer $T_n = 2190 \pm 172$ K, a much hotter nightside than in Table 1. This puts the planet above WASP-14b in Figure 3, with $A_B = 0^{+0.1}$ and $\varepsilon = 0.52^{+0.13}_{-0.12}$ at 1σ. In this case, WASP-12b does not follow the expectation that hotter planets have much shorter radiative times and so larger day–night

contrasts (Cowan & Agol 2011b; Cowan et al. 2012), nor theoretical predictions (Perez-Becker & Showman 2013; Komacek & Showman 2016; Komacek et al. 2017). Instead, the Gaussian decorrelation parameters suggest the planet has a moderate recirculation efficiency despite its high irradiation temperature.

If we remain agnostic about which analysis of the extant data is correct, then WASP-12b's nightside temperature is around 1400–1800 K with a Bond albedo of 0.06–0.22 and a heat recirculation efficiency of 0.21–0.34. New phase curves of the WASP-12 system are needed to determine which of the cases above is most accurate.

The authors thank the anonymous referee for their thorough comments, Kevin B. Stevenson (U. Chicago) for sharing preliminary *Spitzer Space Telescope* data of WASP-43b, and Emily Rauscher (U. Michigan) for sharing GCM light curves of three planets from an in-prep manuscript. The authors also thank Michael Zhang and Heather Knutson (Caltech) for helpful discussions about and improvements to the energy balance model. J.C.S. acknowledges funding as a Graduate Research Trainee at McGill University. This research has made use of the Exoplanet Orbit Database and the Exoplanet Data Explorer at exoplanets.org.

Appendix A
A One-to-one Relation between Phase Offsets and Amplitudes

For a planet on a circular orbit with zonal advection of heat, there is a one-to-one relation between bolometric phase offset and bolometric flux contrast because both depend on a single parameter, recirculation efficiency. To demonstrate this, we use the semi-analytic energy balance model of Cowan & Agol (2011a) and test cases ∼0.02 apart in ε assuming no reflected light (see Appendix C). For each case, we calculate the phase offset and apparent temperature contrast of the disk-integrated flux, as well as for individual gas parcels, as shown in Figure 4. Our results agree qualitatively with three-dimensional general circulation models of super-Earths and mini-Neptunes tested by Zhang & Showman (2017), and they indeed should be universal if heat is zonally advected in the absence of clouds.

A planet's temperature contrast is strongly affected at very low recirculation (dark markers in Figure 4) because it only takes a little heat to raise the temperature of a cold nightside. Although the behavior of individual gas parcels (diamonds) and the disk-integrated light curves (circles) are qualitatively similar, there are two quantitative differences. First, disk integration reduces temperature contrast, as expected given the low-pass nature of the convolution (Cowan & Agol 2008; Cowan et al. 2013). But disk integration also *increases* the phase offset: the hottest disk-integrated region of the planet is East of the hottest gas parcel because parcels heat faster than they cool (Figure 1 of Cowan & Agol 2011a). This means the hot spot is almost never at the center of the planet's brightest hemisphere—one cannot use hot spot offsets and phase offsets interchangeably.

Although the one-to-one correspondence between phase amplitudes and phase offsets was not seen in photometric phase curves (Crossfield 2015), future missions that measure a greater fraction of the thermal emission from short-period planets should allow us to test this prediction directly (e.g., *James Webb Space Telescope*, FINESSE). As noted by Crossfield (2015), deviations from this one-to-one relation would suggest that additional physics—clouds, magnetic fields, etc.—are shaping hot Jupiter

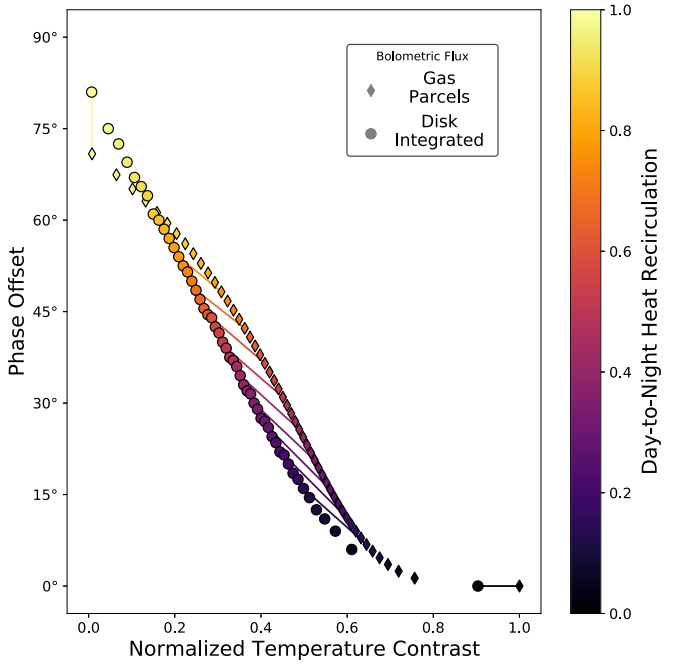

Figure 4. The phase offset vs. apparent temperature contrast, $(T_{\max} - T_{\min})/T_0$, for recirculation efficiencies in ∼0.02 increments (color scale) according to the energy balance model of Cowan & Agol (2011a). This is an upgraded version of the left panel of Figure 9 from Crossfield (2015), which presented an approximate curve for gas parcels interpolated from only a few cases. As the one-to-one relation we predict is technically only valid for *bolometric* phase curves, we omit current observational constraints. Both marker types represent bolometric flux: diamonds show values for individual gas parcels, while circles are for disk-integrated flux. Markers are paired by color; we join select pairs with solid lines. In the radiative equilibrium limit (darkest circle, $\varepsilon = 0$), the disk-integrated temperature contrast is $T_{\rm d} = T_0(2/3)^{1/4}$, as expected. In the limit of efficient zonal heat transport (lightest diamond, $\varepsilon \to 1$), the phase offset of the hot spot approaches $\cos^{-1}(1/\pi) \approx 71.^{\circ}4$. Disk integration decreases the temperature contrast, but *increases* the phase offset. This energy balance model predicts a one-to-one correspondence between bolometric phase amplitudes and offsets, which will be tested with upcoming observations that capture a large fraction of the flux from short-period exoplanets.

phase curves (Agúndez et al. 2012; Perez-Becker & Showman 2013; Rauscher & Menou 2013; Showman & Kaspi 2013).

Appendix B
Phase Curve Precision

Energy budget estimates like those in Table 1 are only as accurate as the phase amplitudes and offsets that constitute them. At a particular order (recall Equation (2)), one can express the phase curve component F_k as the sum of a cosine and sine:

$$F_k \propto \delta_{\rm dn} \cos k\phi + \delta_{\rm ew} \sin k\phi, \tag{4}$$

where $\delta_{\rm dn}$ is the day-to-night phase amplitude and $\delta_{\rm ew}$ is the east-to-west amplitude (we drop the k subscripts for clarity). The two amplitudes are independent variables by Fourier analysis, and their measured uncertainties, $\sigma_{\rm dn}$ and $\sigma_{\rm ew}$, should be similar for full-orbit observations of phase curves. We test this by fitting toy models of phase curves with Equation (4) and find that our amplitude uncertainties are generally within a factor of 2.5. For the published phase curves that used the parameterization above, $\sigma_{\rm dn}$ and $\sigma_{\rm ew}$ differ by 16%–63% in Knutson et al. (2012), <4% in Maxted et al. (2013), and 29% in Zellem et al. (2014), all of which are reasonable.

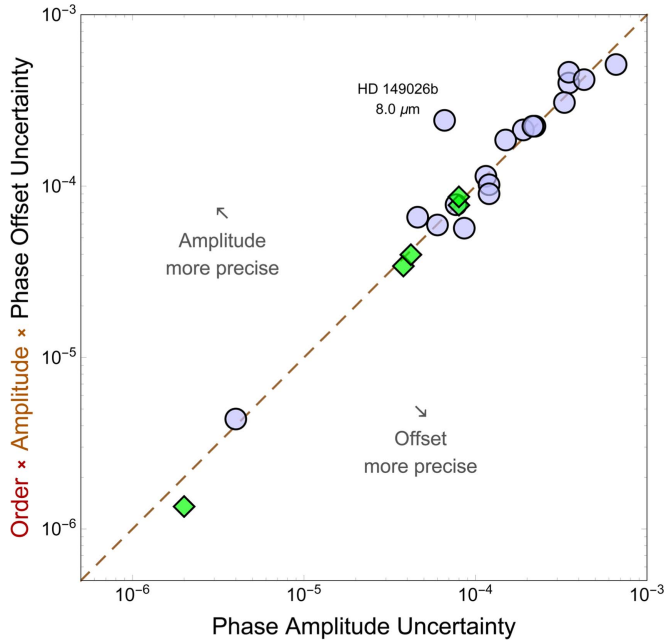

Figure 5. The scaled phase offset uncertainty ($k\delta_k\sigma_\phi$) vs. the phase amplitude uncertainty (σ_δ), motivated by Equation (6). Each marker is a measurement of one planet at one infrared wavelength, where blue circles and green diamonds are first- and second-order data, respectively. Both axes have units of flux and the dashed line shows where these quantities are equal, as expected for sensible σ_δ and σ_ϕ. Only HD 149026b at 8.0 μm has values differing by more than a factor of 2.5, due to a partial phase curve that did not capture the peak flux. Nearly all published phase curves have reasonable phase amplitude and phase offset uncertainties.

Alternatively, the flux component of a planetary system can be parameterized by a cosine with a phase offset:

$$F_k \propto \delta_k \cos\left[k(\phi - \phi_k)\right]. \tag{5}$$

This parameterization has the unfortunate property that the uncertainty on ϕ_k diverges when δ_k is small. This makes it non-trivial to determine whether a given phase amplitude and offset are appropriately precise.[12] The majority of published studies parameterize planetary flux this way.

In order to evaluate the uncertainties $\sigma_{\rm dn}$ and $\sigma_{\rm ew}$, we differentiate the identities $\delta_{\rm dn} = \delta_k \cos k\phi_k$ and $\delta_{\rm ew} = \delta_k \sin k\phi_k$, and rearrange them to obtain

$$\sigma_{\rm dn}^2 - \sigma_{\rm ew}^2 = [\sigma_\delta^2 - (k\delta_k\sigma_\phi)^2]\cos 2k\phi_k, \tag{6}$$

where σ_δ and σ_ϕ are the uncertainties on δ_k and ϕ_k, respectively.

Because we expect its left-hand side to be close to zero, Equation (6) suggests that we compare σ_δ to the product $k\delta_k\sigma_\phi$ for our compiled data, shown in Figure 5. These quantities are reasonable for almost every published observation (i.e., the markers are close to the dashed line). The only outlier is HD 149026b at 8.0 μm (Knutson et al. 2009a), but this is unsurprising as their half-orbit phase curve did not capture the phase curve's peak, so the reported amplitude was merely the observed change in flux.

In short, published phase amplitudes and phase offsets have self-consistent uncertainties, which suggests that including them improves the accuracy of our energy budgets.

[12] This is the same reason it is better to fit for $e\cos\omega$ and $e\sin\omega$ instead of e and ω with radial velocity data.

Appendix C
Apparent versus Effective Temperatures

The view of a planet will affect the disk-integrated bolometric flux one measures, and hence the effective temperature one infers. Visibility is highest at the center of the planetary disk and lowest along the limb; the visibility is zero on the far side of the planet (Cowan et al. 2013). If a planet's hottest locations are directly facing the observer, then that hemisphere will likely appear hotter than its actual effective temperature, and vice versa.

Light curve inversion (Cowan & Agol 2008) provides a means to correct for longitudinal inhomogeneities in brightness and temperature, but this method has not been used to interpret most phase curves. Eclipse mapping can in principle constrain the meridional temperature gradients of the dayside, but so far it has only been applied to one planet in a single spectral band (de Wit et al. 2012; Majeau et al. 2012).

The spatial inhomogeneity of short-period planets therefore presents a challenge to the analysis and interpretation of phase curves: strictly speaking, we need to know the hemispherical effective temperatures to constrain Bond albedo and day–night heat transport, but we can only measure apparent temperatures from a light curve. While apparent temperatures of exoplanets have been discussed before (e.g., Fortney et al. 2006), to our knowledge they have not been explicitly compared to effective temperatures.

For our analysis, we use the semi-analytic energy balance model of Cowan & Agol (2011a). In particular, we consider an idealized hot Jupiter that is on a circular orbit, has no internal heat, reflects no light, and has eastward winds. We numerically solve for this planet's steady-state *bolometric* flux on a grid in latitude and longitude. Next, we assume an equatorial observer and integrate this flux two ways at each orbital phase. In one case, we include the observer's visibility of the planet and so calculate an apparent temperature for that hemisphere,

$$T_{\rm app} = \left(\frac{1}{\pi}\oint V(\mathbf{\Omega})T^4(\mathbf{\Omega})d\mathbf{\Omega}\right)^{\frac{1}{4}}, \tag{7}$$

where $\mathbf{\Omega}$ denotes a location on the surface of the sphere.

In the other case, we use the full flux from every grid point that is visible at all, calculating the hemisphere's effective temperature,

$$T_{\rm eff} = \left(\frac{1}{2\pi}\int T^4(\mathbf{\Omega})d\mathbf{\Omega}\right)^{\frac{1}{4}}, \tag{8}$$

where the integral is only performed on the visible hemisphere of the planet.

Figure 6 shows the temperature ratio for four planetary hemispheres, or orbital phases, as a function of recirculation efficiency.[13] Clearly, apparent and effective temperatures usually differ. At eclipse, a planet's hottest regions are almost always in view for an equatorial observer. We confirm that this leads one to overestimate the dayside effective temperature (yellow solid curve). Nightsides, on the other hand, appear overly cool for recirculation efficiencies up to ≈0.7 (dark solid

[13] Cowan & Agol (2011a) defined recirculation efficiency, $\epsilon \in [0, \infty)$, as the product of a planet's radiative timescale and advective frequency, which differs from $\varepsilon \in [0, 1]$ used by Cowan & Agol (2011b) and in this work. Testing our numerical flux grids, the best-fit function we find to convert between ϵ and ε is:

$$\varepsilon = \frac{\epsilon^b}{c + \epsilon^b},$$

with $b = 1.652$ and $c = 1.828$. We use this equation in Figures 4 and 6.

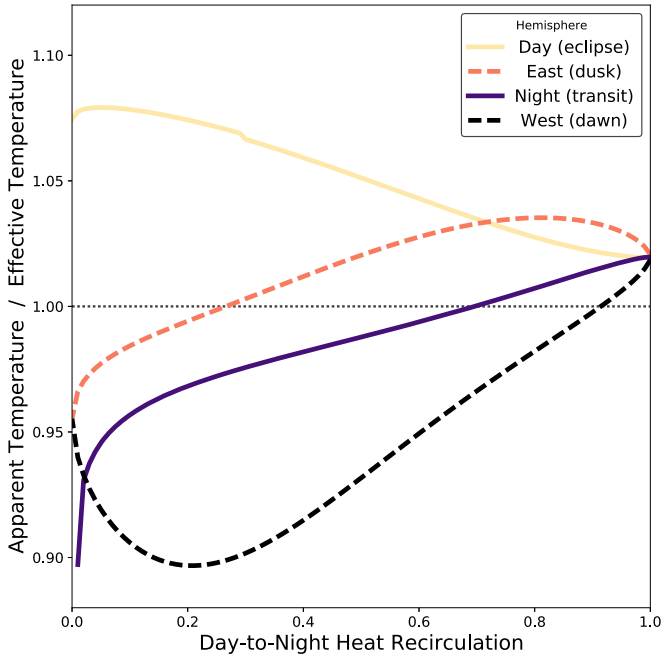

Figure 6. Ratio of apparent temperature (inferred from a *bolometric* light curve) to effective temperature (based on total emitted flux) for four planetary hemispheres, as a function of recirculation. Here, we use the energy balance model for planets on circular orbits in Cowan & Agol (2011a). The dotted line shows where both temperatures are equal. By symmetry, the East and West hemispheres (dashed curves) have the same temperature ratio when $\varepsilon = 0$. As expected, as $\varepsilon \to 1$ all curves approach an identical ratio: $(32/3\pi^2)^{1/4} \approx 1.02$. By estimating recirculation efficiency, one can empirically convert a planet's apparent temperatures into true effective temperatures.

curve). Together, these results show that day and nightside effective temperatures are closer in value than their apparent temperatures. In fact, the real bolometric flux ratios of planets in Figure 3 would be ∼20% larger for HD 189733b to ∼90% for WASP-18b. Furthermore, with perfect recirculation, the temperature ratio for all hemispheres converges to ≈1.02. This is inherent to our model because it does not include poleward heat transport.

If one combines the observed flux from two opposing hemispheres (i.e., values of the light curve at phases 180° apart), then one can try to estimate the effective temperature of the whole planet. In particular, we find the least-biased apparent temperatures are at phases between about 25° and 50° after transit and eclipse (not shown).

We stress that these results are model-dependent. Nonetheless, Figure 6 suggests that naïvely combining apparent temperatures from two diametrically opposite hemispheres of a planet will generally yield the planet's global effective temperature to better than 10%. The scheme of Cowan & Agol (2011b), essentially what we use in the current study, should perform considerably better: it is—by design—accurate in the limits of no heat transport and perfect heat transport.

ORCID iDs

Joel C. Schwartz https://orcid.org/0000-0001-5232-9957
Nicolas B. Cowan https://orcid.org/0000-0001-6129-5699

References

Agúndez, M., Venot, O., Iro, N., et al. 2012, A&A, 548, A73
Allard, F., Homeier, D., & Freytag, B. 2012, RSPTA, 370, 2765
Bechter, E. B., Crepp, J. R., Ngo, H., et al. 2014, ApJ, 788, 2
Bell, T. J., Nikolov, N., Cowan, N. B., et al. 2017, ApJL, 847, L2
Cowan, N. B., & Agol, E. 2008, ApJL, 678, L129
Cowan, N. B., & Agol, E. 2011a, ApJ, 726, 82
Cowan, N. B., & Agol, E. 2011b, ApJ, 729, 54
Cowan, N. B., Fuentes, P. A., & Haggard, H. M. 2013, MNRAS, 434, 2465
Cowan, N. B., Machalek, P., Croll, B., et al. 2012, ApJ, 747, 82
Crossfield, I. J. 2015, PASP, 127, 941
de Wit, J., Gillon, M., Demory, B.-O., & Seager, S. 2012, A&A, 548, A128
Evans, T. M., Aigrain, S., Gibson, N., et al. 2015, MNRAS, 451, 680
Fortney, J. J., Cooper, C. S., Showman, A. P., Marley, M. S., & Freedman, R. S. 2006, ApJ, 652, 746
Han, E., Wang, S. X., Wright, J. T., et al. 2014, PASP, 126, 827
Keating, D., & Cowan, N. B. 2017, ApJL, 849, L5
Knutson, H. A., Charbonneau, D., Cowan, N. B., et al. 2009a, ApJ, 703, 769
Knutson, H. A., Charbonneau, D., Cowan, N. B., et al. 2009b, ApJ, 690, 822
Knutson, H. A., Lewis, N., Fortney, J. J., et al. 2012, ApJ, 754, 22
Komacek, T. D., & Showman, A. P. 2016, ApJ, 821, 16
Komacek, T. D., Showman, A. P., & Tan, X. 2017, ApJ, 835, 198
Line, M. R., Stevenson, K. B., Bean, J., et al. 2016, AJ, 152, 203
Majeau, C., Agol, E., & Cowan, N. B. 2012, ApJL, 747, L20
Maxted, P., Anderson, D., Doyle, A., et al. 2013, MNRAS, 428, 2645
Parmentier, V., Fortney, J. J., Showman, A. P., Morley, C., & Marley, M. S. 2016, ApJ, 828, 22
Perez-Becker, D., & Showman, A. P. 2013, ApJ, 776, 134
Rauscher, E., & Menou, K. 2013, ApJ, 764, 103
Rogers, T. M. 2017, NatAs, 1, 0131
Schneider, J., Dedieu, C., Le Sidaner, P., Savalle, R., & Zolotukhin, I. 2011, A&A, 532, A79
Schwartz, J. C., & Cowan, N. B. 2015, MNRAS, 449, 4192
Showman, A. P., & Kaspi, Y. 2013, ApJ, 776, 85
Stevenson, K. B., Bean, J. L., Madhusudhan, N., & Harrington, J. 2014a, ApJ, 791, 36
Stevenson, K. B., Bean, J. L., Seifahrt, A., et al. 2014b, AJ, 147, 161
Stevenson, K. B., Désert, J.-M., Line, M. R., et al. 2014c, Sci, 346, 838
Stevenson, K. B., Line, M. R., Bean, J. L., et al. 2017, AJ, 153, 68
Wong, I., Knutson, H. A., Kataria, T., et al. 2016, ApJ, 823, 122
Wong, I., Knutson, H. A., Lewis, N. K., et al. 2015, ApJ, 811, 122
Zellem, R. T., Lewis, N. K., Knutson, H. A., et al. 2014, ApJ, 790, 53
Zhang, J., Kempton, E., & Rauscher, E. 2017, arXiv:1711.02684
Zhang, X., & Showman, A. P. 2017, ApJ, 836, 73
Zhou, G., Bayliss, D., Kedziora-Chudczer, L., et al. 2015, MNRAS, 454, 3002